3

Integer Topological Phases: The Integer Quantum Hall Effect and Topological Insulators

The first topological phase to be discovered experimentally was the integer quantum Hall effect (IQHE), which remains one of the most simple and dramatic manifestations of macroscopic quantization. Its subsequent theoretical explanation revealed that even the physics of independent electrons can be remarkably subtle. The Hall effect is a standard probe of conducting materials: when a current I_x runs perpendicular to an applied magnetic field B_z, a transverse voltage V_y builds up. When the material is a two-dimensional electron gas and the magnetic field is sufficiently strong, then there are finite ranges of magnetic field over which the voltage and current satisfy

$$G_{xy} \equiv \frac{I_x}{V_y} = \frac{ne^2}{h}, \tag{3.1}$$

where n is an integer, e is electron charge and h is Planck's constant. Note that all geometric factors drop out for a transverse measurement in two dimensions, so the conductivity σ_{xy} is equal to the conductance G_{xy}.

The remarkable fact is just how well (3.1) is satisfied. The integer quantum Hall effect is the property that, even at nonzero temperature in an imperfect material, a transport quantity is quantized to remarkable precision: the transverse (aka Hall) conductivity on a plateau is $\sigma_{xy} = ne^2/h$, where n is integral to 1 part in 10^9. Taking this experiment as a measure of a fundamental unit of resistance for metrology purposes,[1] the Klitzing constant, one obtains $R_K = h/e^2 \approx 25812.80745\ \Omega$. As a metrological aside, it is amusing to note that what is being measured has changed with time, even though the physical measurement is fundamentally unchanged. In the words of the discoverer (von Klitzing, 2017): "When the QHE was discovered, the SI ohm was more precisely known than the fine-structure constant, which

[1] Until the 1970s, topology seems to have been regarded as entirely without applications. The writer and occasional mathematics teacher Solzhenitsyn (1968) had his surrogate Nerzhin say, "Suddenly he felt sorry for Verenyov. Topology belonged to the stratosphere of human thought. It might conceivably turn out to be of some use in the twenty-fourth century, but for the time being . . . "

https://doi.org/10.1017/9781316226308.004 Published online by Cambridge University Press

is why the first QHE publication was entitled 'New method for high-accuracy determination of the fine-structure constant based on quantized Hall resistance.' However, this title will be wrong when the new SI features a fixed value for the von Klitzing constant. When that happens [as it has in 2019], the manuscript's original title, 'Realization of a resistance standard based on natural constants,' rejected at the time by Physical Review Letters, will turn out to be more appropriate."

This precision results because the transport is determined by a topological invariant, as stated most clearly in work of Thouless. Consequently we say that Thouless-type topological order is present in phases where a response function is determined by a topological invariant. The gapless edge or surface states that often exist at the boundary between a Thouless-type phase and an ordinary insulator are a consequence of this topological response. Another type of topological order (Wen-type) is present in phases with fractional particles, such as fractional quantum Hall phases and the quantum dimer model (Chapter 5).

The importance of Thouless-type topological order for condensed matter physics has expanded greatly in the past few years with the discovery of topological phases in which spin-orbit coupling, rather than magnetic field, produces the new phase. These phases exist in both two and three dimensions, unlike the IQHE which is essentially two-dimensional. They have unusual edge and surface states that we use to introduce their physics as measured in experiments, leading into the deeper theoretical analysis in the following chapter. The easiest way to picture the 2D topological insulator phase is as two copies of the IQHE in which spin-up and spin-down electrons (along some axis) feel opposite magnetic fields from the spin-orbit coupling.

This is also known as the quantum spin Hall effect (QSHE) because in this ideal case it supports a spin transport phenomenon analogous to (3.1). However, there are important and subtle differences between the QSHE and a doubled IQHE, and the theoretical explanation of these in terms of a new kind of topological invariant by Kane and Mele (2005b) triggered an avalanche of theoretical developments that continues to the time of this volume's writing. We will explain the basic idea of their work and its relation to the *charge* transport measurement at Würzburg that gave the first experimental evidence for the QSHE (Koenig et al., 2007).

A rather important consequence of Kane and Mele's work was that theorists, in trying to understand the new topological invariant, realized that it had a fully three-dimensional analogue (Fu et al., 2007; Moore and Balents, 2007; Roy, 2009). The term topological insulator was coined to describe this phase (Moore and Balents, 2007) because there is no longer any quantized transport quantity like the Hall effect, at least in the material's native state; what exactly is quantized is a kind of magnetoelectric effect. The three-dimensional topological insulator

resulting from this invariant was soon observed experimentally, but not by a transport experiment; instead its distinctive surface state was imaged in a photoemission experiment (Hsieh et al., 2008). The relative ease of making and measuring 3D topological insulators has led to an explosion of experimental work. A summary of the early history of the 2D and 3D topological insulators with examples of key materials is Moore (2010).

In this chapter we seek instead to give physical arguments and examples for the topological properties that give rise to the states we discuss, deferring a more mathematical discussion to the following chapter on wavefunction geometry and Berry phases. The essential aspects of these states can be understood from fairly simple assumptions about magnetic fields, spin-orbit coupling, disorder, and time-reversal symmetry. At a deeper level, the topological properties are described by an invariant resulting from integration of an underlying Berry phase. It turns out that the Berry phase can be rather important even when it is not part of a topological invariant. In crystalline solids, the electrical polarization, the anomalous Hall effect, and part of magnetoelectric polarizability also derive from Berry phases of the Bloch electron states, as described in Chapter 4.

First we give some background for the original quantum Hall discovery by Dorda, Pepper, and von Klitzing in 1980, which triggered a flood of developments continuing to the present day, and for the more recent discovery of topological insulators in two and three dimensions. We cover the classic explanation by Laughlin for the precision of quantization in the IQHE, then in later sections explain the more recently discovered integer topological phases with reference to simple tight-binding models on the honeycomb lattice that were important in their understanding. The chapter closes with an important physical example that combines several concepts from Chapter 2: skyrmions in the quantum Hall effect, which add a dose of quantum mechanics to the theory of topological defects.

3.1 IQHE: Basic Phenomena and Theory

What does it mean to say that electrons move only in two dimensions? Imagine a perfectly planar interface between two insulators so that the electronic eigenstates decompose into products of a wavefunction in the normal direction z and a plane wave in the xy plane: $\psi(x, y, z) = \phi(z)e^{i(k_x x + k_y y)}$. If there is a single bound state for electrons at the interface, and if the temperature is much less than the energy separation between this bound state and other transverse wavefunctions, then electronic motion in the z direction is frozen out: the electron is perfectly two-dimensional with respect to low-energy processes that are unable to promote the electron to a different z state. Even if a finite number of bound states (subbands)

https://doi.org/10.1017/9781316226308.004 Published online by Cambridge University Press

are occupied, the essential features remain two-dimensional because the electronic motion in the normal direction is strongly quantized. The technique of modulation doping in molecular beam epitaxy allows the creation of 2D electron gases (2DEGs) with extremely long electron mean free paths, comparable to the sample size (Box 3.2).

The original, nonquantized Hall effect is a valuable probe of materials because, in a simple Drude model of 2D transport with a single relaxation time τ, a Hall ratio R_H can be formed in which the relaxation time drops out and only the density and charge of the carriers survives (Ashcroft and Mermin, 1976):

$$R_H = \frac{V_y}{I_x B} = \frac{1}{n_{2D} e}. \tag{3.2}$$

Here the areal density of carriers is n_{2D}. Then the Hall conductivity is

$$\sigma_{xy} = \frac{n_{2D} e}{B}. \tag{3.3}$$

The quantized values $\sigma_{xy} = ne^2/h$ then correspond to an electron density

$$n_{2D} = \frac{neB}{h} = \frac{n}{2\pi \ell^2}, \tag{3.4}$$

or n electrons per (single-electron) flux quantum $\frac{eB}{h}$. We have introduced the magnetic length $\ell = \sqrt{\hbar/eB}$.[2]

The inverse areal density $2\pi\ell^2$ is known to be special from a classic calculation in nonrelativistic quantum mechanics (Section 2.2). A 2D electron moving in a perpendicular magnetic field has, ignoring the Zeeman coupling, highly degenerate electron energy levels spaced by $\hbar\omega_c$, where $\omega_c = eB/m$ is the classical cyclotron frequency (the angular frequency at which an electron orbits under the Lorentz force of the magnetic field). These Landau levels have a degeneracy which scales with the area of the system; each Landau level contains one electronic state per flux quantum. So the occurrence of features in transport when the chemical potential passes through a Landau level because of a change in the magnetic field is not very surprising.

What requires explanation is that the plateaux have nonzero width, that is, that σ_{xy} is flat on a plateau to a tremendously good approximation. It is as though the state of the system is not changing at all, even as the magnetic field changes by a significant percentage. The existence of plateaux is even more surprising when one realizes that in the calculation above of a perfectly clean system, the electrical field E_y associated with the transverse voltage can be made zero by a Lorentz transformation to the frame moving with velocity E_y/B. In this frame the electrons are

[2] This is one of several places where our use of SI units, following most experimental papers, may cause confusion when comparing to other sources using Gaussian-CGS units. Conversions are given in Table A.1 of the appendix.

https://doi.org/10.1017/9781316226308.004 Published online by Cambridge University Press

stationary, which implies that the Hall ratio in the original frame is exactly proportional to $1/B$ with no plateaux (Eq. 8.10)! The current theoretical understanding is that the IQHE system is in fact changing on a plateau, but that the only changes involve localized electronic states that do not contribute to transport (see Chapter 8). In a moment we will repeat a classic argument of Laughlin for what happens on a quantum Hall plateau.

In order to make the following argument more concrete, it is worthwhile to introduce a basis for wavefunctions in the lowest Landau level. For problems with rotational symmetry, a nice basis is ($z = x + iy$)

$$\psi_m(z) = \frac{\left(\frac{z}{\sqrt{2}\ell}\right)^m \exp(-|z|^2/4\ell^2)}{\sqrt{2\pi\ell^2 m!}}, \tag{3.5}$$

the $n = 0$ case of the form given in Section 2.2, where $m = 0, 1, \ldots$. The exponential factor keeps the electrons confined in the vicinity of the origin; more precisely, a quick calculation shows that the magnitude $|\psi_m|^2$ is maximized at radius $r = \ell\sqrt{2m}$, and the mean squared radius is

$$\langle r^2 \rangle_m = 2(m+1)\ell^2. \tag{3.6}$$

As a check, the number of states within a ring of large radius R is approximately $R^2/(2\ell^2) = \pi R^2/(2\pi\ell^2)$, confirming that the areal density is $1/(2\pi\ell^2)$. We will want to study in a moment how the filled Landau level made up of these states responds to an applied electric field, but it may be useful first to review the simpler problem of a particle moving on a ring pierced by a magnetic flux in Box 3.1. The key feature is that an integer number of flux quanta can be gauged away and do not modify the spectrum. The connection is that we will find it useful to generate electric fields through a time-varying flux through a hole in the Landau level, and there must be a relationship between the original state and the final state once an integer number of flux quanta have been added.

Box 3.1 One Particle on a Ring Pierced by Magnetic Flux

A famous consequence of the way electromagnetic fields appear in quantum mechanics is the Aharonov-Bohm effect: even if there is no magnetic field in some region of space, a particle moving in that region can notice the effects of a magnetic field elsewhere. In the simplest case, this effect is a consequence of the fact that the vector potential **A** rather than the magnetic field **B** appears in the Schrödinger equation. Considering a particle moving on an idealized one-dimensional loop (Figure 3.1a) allows us to see, however, that at certain values of the magnetic flux through the loop, the Aharonov–Bohm effect on physical quantities disappears.

https://doi.org/10.1017/9781316226308.004 Published online by Cambridge University Press

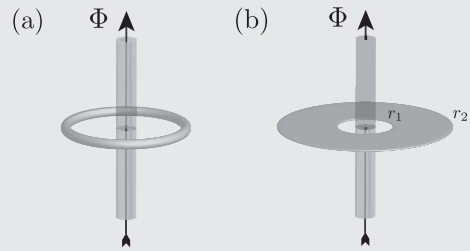

Fig. 3.1 (a) Insertion of magnetic flux Φ through a solenoid passing through a ring modifies the wavefunctions and energies as described in Eq. 3.11. (b) Geometry of Laughlin pumping. The flux is now inserted through a solenoid inside the inner radius r_1 of a two-dimensional electron gas confined to an annulus or Corbino disk. If the electrons are in an integer quantum Hall state, the effect of adiabatically pumping flux $\Phi_0 = h/e$ will be to shuttle an integer number of electrons from the inner edge at radius r_1 to the outer edge at r_2 or vice versa, via the process shown in Figure 3.2.

Without flux, the Hamiltonian on the ring is just

$$H = -\frac{\hbar^2}{2m}(\partial_x \psi)^2, \tag{3.7}$$

where x is a coordinate along the ring: x and $x + 2\pi R$ therefore represent the same physical point, where R is the radius of the ring. So the energy eigenstates are plane waves e^{ikx}, with energies $\hbar^2 k^2/(2m)$, but we must restrict the values of k to

$$k_n = \frac{2\pi n}{2\pi R} = \frac{n}{R}, \quad n \in \mathbb{Z} \tag{3.8}$$

in order for the periodicity condition to be satisfied.

How is this modified when a magnetic flux Φ pierces the ring, for example in an infinitesimally narrow solenoid through the ring's center? The line integral of the vector potential around the ring is the magnetic flux:

$$\oint A_x \, dx = \int B \, dA = \Phi. \tag{3.9}$$

The Hamiltonian now takes the form, supposing that the particle is an electron with charge $-e$,

$$H = \frac{1}{2m}(-i\hbar\partial_x + eA_x)^2, \tag{3.10}$$

which implies that the energies are modified to

$$E_n = \frac{\hbar^2}{2m}\left(\frac{n}{R} + \frac{e\Phi}{2\pi R\hbar}\right)^2 = \frac{\hbar^2}{2mR^2}\left(n + \frac{\Phi}{\Phi_0}\right)^2. \tag{3.11}$$

https://doi.org/10.1017/9781316226308.004 Published online by Cambridge University Press

Here $\Phi_0 = h/e$ is the single-electron flux quantum. We can view the flux as having induced a phase shift on going around the ring through the Aharonov–Bohm effect, which causes the allowed values of kinetic momentum to shift.

However, we see that if the applied flux Φ is an integer multiple of the flux quantum Φ_0, the spectrum has not changed at all. It might seem as though the wavefunctions have changed, but this change is not physically observable as it can be removed by a gauge transformation that changes both A and the wavefunction phase. We say that an integer number of flux quanta that do not penetrate the regions where electrons are present can be gauged away, as they do not affect the spectrum or other observable quantities; it is only the fractional part of fluxes that generate observable Aharonov–Bohm phases. The concept of Laughlin pumping is essentially that, even if the spectrum with one flux quantum is the same as that at zero flux, there could be a nontrivial evolution called spectral flow as the flux is changed. Even in this ring example we can see, starting with the $n = 0$ state, that its energy would smoothly increase as flux was inserted until at one flux quantum, it had the energy of what was originally the $n = 1$ state.

The other remark we make about this model is that at half-integer fluxes $\Phi = \pm\frac{\Phi_0}{2}, \pm\frac{3\Phi_0}{2}, \ldots$ the spectrum has a twofold degeneracy. We can view this degeneracy as reflecting a kind of time-reversal symmetry: without changing the flux through the ring, there are always right-moving and left-moving states at the same energy. At these fluxes, the phase factor induced on moving around the circle is just -1, and hence real, unlike the complex phases at other noninteger flux values. A consequence is that if we require that the spectrum be invariant under taking the complex conjugate of the wavefunctions, which transforms k to $-k$, without changing the flux, then there are only two fluxes that qualify: integer flux and half-integer flux (note that all integer fluxes are indistinguishable from each other by the above argument, and likewise for half-integer fluxes). A way to make this argument more abstract is that the set of integer fluxes is invariant under $\Phi \to -\Phi$, but so is the set of half-integer fluxes. The idea that a system with periodic variable (here Φ) that flips sign under some symmetry might permit exactly two inequivalent classes turns out to be useful later on, for example in the discussion of electrical polarization and the quantized magnetoelectric effect in Section 4.5.

Consider a Corbino disk geometry where a material is present in an annulus $r_1 < r < r_2$. We wish to consider the Hall current in this material between the inner and outer edges when an electromotive force is applied by changing the flux through a solenoid located at the origin (Figure 3.1b). We assume that the flux Φ is increased from zero adiabatically, that is, at sufficiently low frequency that there are no excitations across the gap. The gauge invariance of the Schrödinger

https://doi.org/10.1017/9781316226308.004 Published online by Cambridge University Press

equation implies that when the flux through the solenoid reaches one flux quantum, the quantum-mechanical eigenstates are equivalent via a gauge transformation to those at zero flux.

Laughlin argued that the net result of the adiabatic flux increase must have been to transfer an integer number of electrons, possibly zero, from one edge of the annulus to the other. This is physically plausible if no electronic states span the annulus, so that the question of how many electrons are in the annulus is well defined up to edge contributions; indeed the quantization of the IQHE is expected to break down at sample widths comparable to a magnetic length, when wavefunctions from one edge tunnel appreciably to the other. If an integer n electrons are transferred by an increase of one flux quantum h/e, then the Hall conductance averaged over the period of the flux increase can be computed by computing the current flow across a ring of radius r anywhere in the annulus. Writing Φ for the flux through the annulus, and using Maxwell's equations to relate the flux change to the induced electric field, we obtain

$$\frac{\int_0^T j_r\, dt}{T E_\theta} = \frac{ne/2\pi r}{(T/2\pi r)\frac{d\Phi}{dt}} = \frac{ne}{h/e} = \frac{ne^2}{h}. \tag{3.12}$$

The strength of this argument is that it applies as long as the Fermi level lies in a mobility gap, that is, localized states at the Fermi level do not affect the premise that an integer number of charges be transferred. The actual behavior of electrons in a magnetic field and disorder potential is discussed in some detail in Chapter 8.

To understand concretely how the flux induces charge transport, let us consider how the solenoid modifies the wavefunctions (3.5). Note that if we really took these wavefunctions to model our system exactly, then the annulus of occupied states has simply shifted outward, that is, the system has moved. If the final state is to be the same as the initial state, then there must be reservoirs of charge at the inner and outer edges, able to transfer electrons into and out of the annulus that is in the QHE regime. These must be gapless because the electron transfer occurs adiabatically. The importance of this gapless edge state was pointed out in an important paper by Halperin (1982). A model of how the edge state arises is to think about the evolution of states shown in Figure 3.2, and note the gapless spectrum near the edge; one can think about these discrete modes as arising from quantizing edge ripples on an incompressible droplet. We will have much more to say about these edge states later, as the primary means of learning about the order in integer and fractional quantum Hall states is via edge measurements.

Transport in the Laughlin picture occurs by a very counterintuitive process. Normally transport of independent electrons in a solid is described in terms of

https://doi.org/10.1017/9781316226308.004 Published online by Cambridge University Press

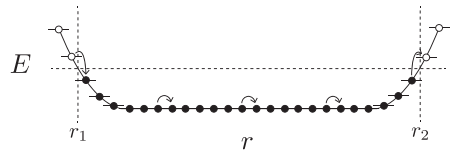

Fig. 3.2 Adiabatic transport by pumping in the quantum Hall effect. Suppose that a weak confining potential is added to the lowest Landau level so that the electrons are trapped in an annulus $r_1 < r < r_2$. The Fermi level (horizontal dotted line) separates occupied states (solid circles) from empty states (open circles). For a weak potential, it is sufficient to picture the symmetric-gauge eigenfunctions as unchanged and localized at different values of the radius as shown. As a flux through the inner circle of the annulus is adiabatically increased from zero to one flux quantum $\Phi_0 = h/e$, the eigenstates smoothly shift over as indicated by the arrows. The effect of the pumping cycle is to transport one electron from the inner edge at r_1 to the outer edge at r_2.

the occupancy of single-electron states changing; an electron hops between different states in roughly the same way as a person climbing stairs moves between stairs. The adiabatic transport taking place in the Laughlin argument as the flux is increased is like an escalator or baggage carousel: the states are continuously evolving and carrying the electrons with them (Figure 3.2). Whether adiabatic or ordinary transport is taking place in a given quantum Hall experiment is a subtle issue because of the gapless edge states described above. Transport between two reservoirs connected by an edge state can be understood in the conventional picture of electronic occupancies, while transport between reservoirs connected by a gapped region, as in the Laughlin argument, requires that the states evolve, not just their occupancies.

In the above discussion of the quantum Hall effect, we ignored entirely the effects of band structure in the underlying material. This is a reasonable approximation for traditional semiconductor 2DEGs in the following sense. For realistic laboratory magnetic fields, the magnetic flux through one unit cell is much smaller than a flux quantum, so a description in terms of Bloch wavepackets is acceptable (Ashcroft and Mermin, 1976). For typical 2DEG densities, only the bottom or top of the 2D band is appreciably occupied and the band physics can be captured simply by an effective mass. Some additional physics and history of ultraclean 2DEGs, including the key advance of modulation doping, is discussed in Box 3.2. These assumptions do not apply when the magnetic field is replaced by the spin-dependent forces that give rise to topological insulators, as those forces vary significantly on the length scale of a unit cell. Hence we will need to develop an alternate picture of the IQHE even to describe the simplest model of the 2D topological insulator, which is as two oppositely directed copies of the IQHE.

Box 3.2 Modulation Doping

Progress in sample growth and measurement techniques are as crucial for pushing back the boundaries of knowledge as ideas and theories. One notable instance of the former is the invention of modulation doping, which lowered the level of electrostatic disorder in the two-dimensional electron liquid to a point where a many-body phenomenon as delicate as the FQHE could be observed. The impact of that invention is hard to overstate – the resulting high-mobility semiconductor heterostructures have found their place in innumerable applications including semiconductor lasers and high-electron-mobility transistors (HEMTs).[a]

The need for modulation doping arises because semiconductors such as gallium arsenide (GaAs) need to be supplied with carriers (electrons or holes) in order to have interesting physics at temperatures well below their intrinsic band gap. The dopant ions such as aluminum that are used to donate these carriers serve as potential scatterers as their ionic potentials are necessarily different from those of the atoms they substitute. (In practice the randomness in the locations of these dopant atoms cannot entirely be

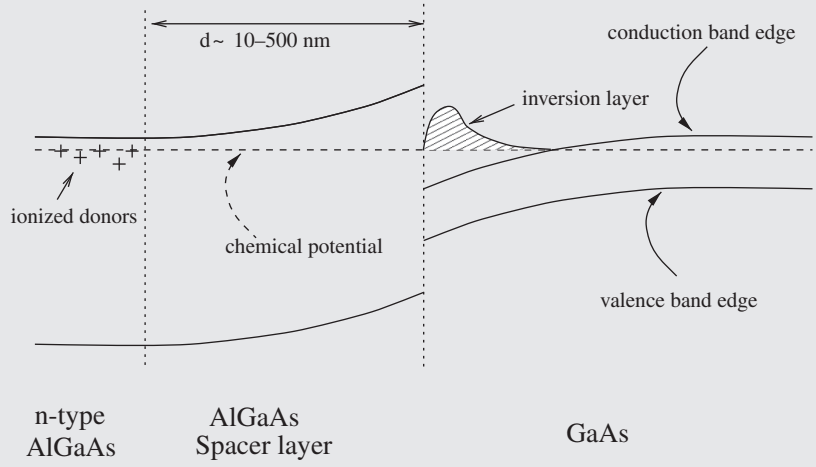

Fig. 3.3 Modulation-doped GaAs heterostructure. The structure is two-dimensional, and the horizontal axis denotes the layer-by-layer growth direction in real space. The vertical direction shows the energies of conduction (top) and valence (bottom) bands. The mobile carriers (electrons, in this case) exist in a thin inversion layer at an interface, where the conduction band dips below the chemical potential. The dopant ions, whose ionization contributes these carriers, are deposited in layers some distance away, so the disorder potential they contribute is rather suppressed by the intervening charge-neutral spacer layer. From Moessner (1997).

https://doi.org/10.1017/9781316226308.004 Published online by Cambridge University Press

eliminated.) At low temperatures where electron-phonon scattering is irrelevant, these dopant potentials are the primary source of resistivity.

Modulation doping takes advantage of the flexibility of layer-by-layer deposition of atoms using techniques such as molecular beam epitaxy. This allows separating the donor layer spatially from the 2DEG, which decreases the disorder potential *exponentially* in the layer separation.

A modulation-doped quantum well (Figure 3.3) is grown layer by layer via molecular beam epitaxy, with a spacer layer separating the dopants from the carriers in the quantum well. That this is useful in suppressing the disorder potential follows from Poisson's equation $\nabla^2\phi(\mathbf{r}) = \rho_c$, which connects the electric potential ϕ with the charge density ρ_c. In the spacer layer, $\rho_c = 0$, so that the Fourier transform of the potential satisfies

$$\mathbf{k}^2\phi_{\mathbf{k}} = (k_\perp^2 + k_\parallel^2)\phi_{\mathbf{k}} = 0 \Longrightarrow k_\perp^2 = -k_\parallel^2. \tag{3.13}$$

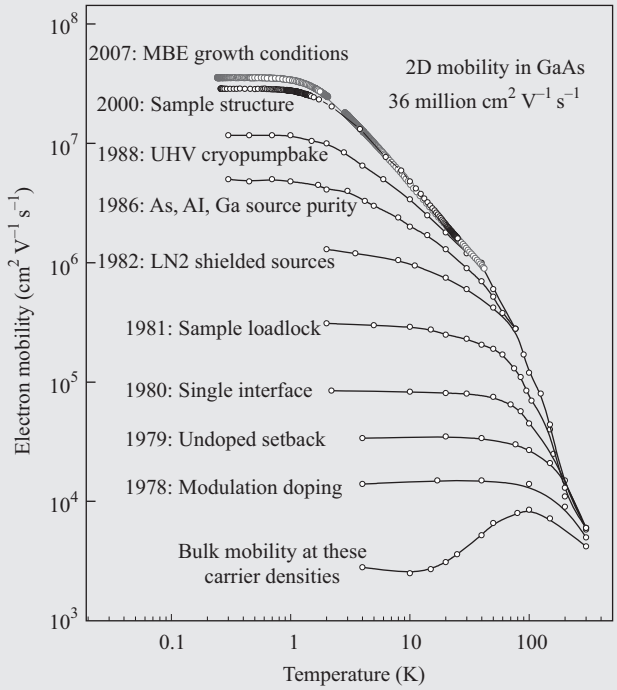

Fig. 3.4 Increase of low-temperature mobility in two-dimensional electron liquids with time. The "bulk" curve denotes a uniformly doped GaAs sample, while "undoped setback" precedes the introduction of modulation doping. Increased mobility was a primary cause of successive discoveries in quantum Hall physics, including the first odd-denominator fraction in 1982 and the first even-denominator fraction in 1989. From Schlom and Pfeiffer (2010). Reprinted with permission by Nature Publishing Group.

https://doi.org/10.1017/9781316226308.004 Published online by Cambridge University Press

This means that a variation of the potential with wavevector $k_\parallel$ in the plane must decay exponentially, with decay constant $\kappa_\perp = k_\parallel$: short-wavelength fluctuations decay faster than long-wavelength ones.

The carriers in the quantum well can thus have extremely long mean free paths, leading to the high mobilities shown in Figure 3.4. Major physics discoveries have occurred as a consequence of these increases in mobility. Graphene, a quite different type of two-dimensional electron gas, has similarly seen new correlated states emerge as a result of increases in mobility. Here the mobility increases were achieved using two techniques: by finding good substrates, such as boron nitride, and by suspending the graphene (i.e., not using a substrate at all).

[a] The textbook Ashcroft and Mermin (1976) is a good reference for the basic physics of such heterostructures.

3.2 Two Lattice Models of the IQHE, and Chern Number

Someone new to solid-state physics might be skeptical that the Landau level wavefunctions described in (3.5), for an electron moving in a constant magnetic field in free space, remain relevant when the electron also feels a periodic potential from the crystalline background. The Hofstadter model is possibly the simplest example of how to incorporate the orbital effect of a magnetic field in a model of a crystal. Its full behavior is quite rich, but we will concentrate here on its topological aspects and on recovering Landau level physics when the magnetic field is weak.

Consider free electrons moving on the square lattice with bond length a, and ignore spin for now. The tight-binding Hamiltonian with nearest-neighbor interactions is, in zero magnetic field,

$$H = -\sum_{\langle ij \rangle} t(c_i^\dagger c_j + c_j^\dagger c_i), \tag{3.14}$$

where $t > 0$ is the hopping matrix element and the sum is over nearest-neighbor sites i and j. With periodic boundary conditions on an $N \times N$ lattice, introduce the Fourier-transformed plane wave operators

$$c_{\mathbf{k}}^\dagger = \frac{1}{\sqrt{N}} \sum_i c_i^\dagger e^{-i\mathbf{k}\cdot \mathbf{r}_i}, \tag{3.15}$$

where the components of $\mathbf{k} = (k_x, k_y)$ are integer multiples of $\frac{2\pi}{Na}$, and $\mathbf{r}_i$ is the location of site i. Then the Hamiltonian is diagonalized as

$$H = \sum_{\mathbf{k}} \epsilon_{\mathbf{k}} c_{\mathbf{k}}^\dagger c_{\mathbf{k}} \tag{3.16}$$

https://doi.org/10.1017/9781316226308.004 Published online by Cambridge University Press

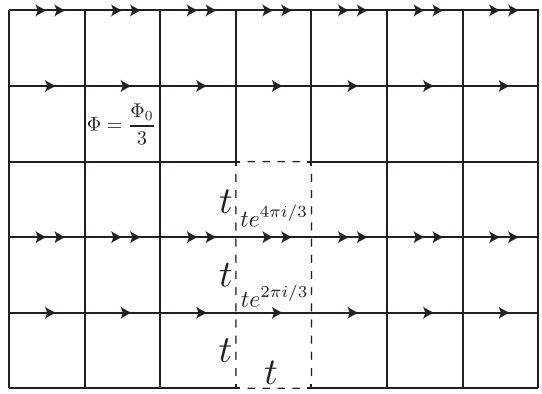

Fig. 3.5 The Hofstadter model: one particle hopping on a square lattice with a magnetic flux Φ through each plaquette. Here $\Phi = \Phi_0/3$, and we have chosen Landau gauge with the vector potential along $\hat{\mathbf{x}}$ and varying with y. All vertical bonds have just the original zero-field hopping t. Horizontal bonds take one of three possible values, denoted by zero arrows, one arrow, or two arrows. A unit cell or supercell of the system at this flux (dotted lines) contains three original unit cells.

with the eigenenergies $\epsilon_{\mathbf{k}} = -2t(\cos k_x a + \cos k_y a)$. This system has one site per unit cell and hence one band in the first Brillouin zone.[3]

The Hofstadter model (Hofstadter, 1976) is obtained by adding a uniform perpendicular magnetic field $\mathbf{B} = B\hat{\mathbf{z}}$ to this tight-binding model, with flux Φ per unit cell (Figure 3.5). How do we incorporate such a magnetic field into the tight-binding model? Moving an electron around any plaquette should pick up a phase Φ through the Aharonov-Bohm effect. That is accomplished by changing the Hamiltonian in (3.14) to incorporate a phase into the hopping amplitudes,

$$H = -\sum_{\langle ij \rangle} \left[t \exp\left(i \frac{2\pi}{\Phi_0} \int_{\mathbf{r}_j}^{\mathbf{r}_i} \mathbf{A} \cdot \mathbf{dr} \right) c_i^\dagger c_j + \text{h.c.} \right]. \tag{3.17}$$

Here $\mathbf{A}$ is the electromagnetic vector potential created by the magnetic field. We remark in passing that this phase factor resulting from integrating a gauge potential along a line in real space is known as a Wilson loop and has some important applications in practical methods for calculating topological invariants.

For general values of the flux, the Hofstadter Hamiltonian (3.17) is quite challenging to solve. When the flux is a rational multiple of the single-electron flux quantum,

$$\Phi = \frac{p}{q}\Phi_0 = \frac{p}{q}\frac{h}{e}, \quad p, q \in \mathbb{Z}, \tag{3.18}$$

[3] A puzzle for students, of relevance to the high-temperature cuprate superconductors, which exist on this lattice: what is the shape of the Fermi surface at half-filling?

https://doi.org/10.1017/9781316226308.004 Published online by Cambridge University Press

then the system still has a finite unit cell and Bloch eigenstates. Note that $p \ll q$ for achievable magnetic fields in crystals, since one flux quantum through a typical unit cell of a few angstroms on a side would be achieved only at fields of order 10^5 Tesla. The importance of the commensurability condition (3.18) can be seen by working in the Landau gauge, with vector potential

$$\mathbf{A} = (-By, 0, 0), \quad \nabla \times \mathbf{A} = B\hat{\mathbf{z}}, \quad B = \frac{\Phi}{a^2}. \tag{3.19}$$

This leads to phase factors on horizontal bonds that indeed satisfy the expected Aharonov-Bohm relation. Let us take $\Phi = \Phi_0/3$ for simplicity as shown in Figure 3.5. The hopping amplitudes on horizontal bonds are arranged in a repeating sequence of period 3 with values $(-t, -te^{2\pi i/3}, -te^{4\pi i/3})$, with the amplitude to hop from right to left being the complex conjugate of the amplitude to hop from left to right. Because the new unit cell or supercell is three times as large as before, and contains three sites, we can expect three bands in a Brillouin zone that is one-third as large as in the case of zero field.

By the same process, if we looked at smaller commensurate fluxes $\Phi = \Phi_0/n$, we would have n bands to consider. Calculating the energies of the Bloch eigenstates is not too difficult, but these energies are not the most important facts about the model. Let us suppose that the bands occupy disjoint regions in energy, so that when some bands are filled but not others, we have a band insulator. Is this band insulator different from the standard insulators one learns about in a first course?

The answer is yes, and in fact these are our first examples of topologically nontrivial bands, in this case bands of nonzero Chern number, which is a fancy way of saying that they have something in common with the Landau levels we found for a free electron. Indeed, as n becomes very large, the bands of the Hofstadter model become flat in energy, and the lowest bands can be viewed as the first few Landau levels. This makes sense if we think about the lowest bands as made out of the lowest-energy states of the zero-field model, which are close to free electron states, for example, they have a similar quadratic dispersion obtained by expanding around the minimum of the band structure.

Even at $n = 3$, there is something topological about the bands obtained by solving the Hofstadter model, which is our first example of a topological band structure. The eigenstates and eigenenergies can be found by diagonalizing the three-by-three Bloch Hamiltonian. The detailed values of the energies are not very important, but for illustration, the lowest band's energy is found to be, setting the lattice spacing $a = 1$:

$$E(\mathbf{k}) = 2\sqrt{2}\cos[\phi(\mathbf{k}) + 2\pi/3], \tag{3.20}$$

https://doi.org/10.1017/9781316226308.004 Published online by Cambridge University Press

where

$$\phi(\mathbf{k}) = \frac{1}{3}\cos^{-1}\left[-\frac{\cos(3k_x)+\cos(3k_y)}{2\sqrt{2}}\right], \tag{3.21}$$

in which the symmetry between x and y is manifest, even if it was broken in the wavefunctions by our gauge choice. More important for our purposes is the fact that this lowest band, for example, responds to an inserted flux in the same way as a Landau level.

More generally, we can associate an integer-valued topological invariant called the Chern number or TKNN integer with each band in the Hofstadter model. That integer has a physical meaning – it describes how much that band, if it is filled with electrons, contributes to the IQHE:[4]

$$\sigma_{yx} = \frac{e^2}{h}\sum_{\text{occ } i} C_i, \quad C_i = \frac{1}{2\pi}\int \mathcal{F}^i \, d^2k. \tag{3.22}$$

Here $C_i \in \mathbb{Z}$ is the Chern number of band i. The integrand $\mathcal{F}^i$ is known as the Berry curvature or Berry flux of the Bloch states in band i and takes the form (cf. Eq. 2.9)

$$\mathcal{F}^i = (\nabla_k \times \boldsymbol{\mathcal{A}}^i)_z, \quad \mathcal{A}^i_\lambda = i\langle u^i | \partial_\lambda u^i \rangle. \tag{3.23}$$

Here we have broken our rule of not introducing microscopic formulae until Chapter 4, in addition to trusting the reader to distinguish between band index i and $i = \sqrt{-1}$, but the historical impact of Eq. 3.22 is sufficient to warrant an exception. At a conceptual level, suffice it to say for now that something about how the wavefunctions wind with momentum leads to an effective gauge field $\mathcal{A}$ in the two-dimensional Brillouin zone, and a topological integer characterizing each band.

The Hofstadter problem with $n = 3$ discussed above has Chern numbers $C_1 = 1, C_2 = -2, C_3 = 1$ for the three bands. In general, for n odd this pattern still obtains: the total Chern number is zero, and all bands have Chern number 1 except for the band in the middle. For even n, only the two bands in the middle have Chern numbers different from one; their Chern numbers are equal and make the total of Chern numbers for the entire band structure equal to 0.

The remarkable expression (3.22), found by Thouless, Kohmoto, den Nijs, and Nightgale in a seminal 1982 paper (Thouless et al., 1982), connects the topology of wavefunctions to a physical observable. Part of their motivation was to explain how the quantization predicted by Laughlin's pumping argument can be recovered

[4] The σ_{yx} instead of σ_{xy} in this formula is not a typo but a deliberate minus sign; it originates in the existence of two sign conventions for the Berry curvature and hence C_i. TKNN defined the Berry connection with a minus sign relative to the contemporaneous definition by Berry, which we have followed here. Our convention, which is also that of Vanderbilt (2018), makes natural the expression for polarization in Chapter 4.

by relatively standard means, namely, calculation of σ_{xy} starting from the general Kubo linear-response expression for σ_{xy}. We will derive (3.22) and give an expression for C_i in terms of the Bloch wavefunctions in the following chapter.

For now, we state some basic facts without proof. Each isolated band has a Chern number, and when two bands touch, their total Chern number remains a well-defined integer even though each individual band may not have its own Chern number. We have discussed Chern number here for a two-dimensional band structure, but each band in a three-dimensional band structure has three Chern numbers, related to xy, yz, and xz planes in the Brillouin zone. Finally, the Chern number and the IQHE it predicts remain well-defined concepts even when interactions are added between the electrons, as long as the ground state remains nondegenerate. Without a magnetic field or magnetism in a material, there is a symmetry known as time-reversal symmetry, discussed in the following section, that forces all $C_i = 0$.

The importance of time-reversal symmetry will start to be evident in the second lattice model we discuss, which was introduced by Haldane as a model of the IQHE and Chern bands without a macroscopic magnetic field. As in the Hofstadter problem, we start with a band structure that is not topological. This is the nearest-neighbor hopping model on the honeycomb lattice, a well-known model for graphene, which we introduced in Section 2.5. An illustration of a two-dimensional linear dispersion characteristic of a Dirac point like the ones in graphene is also provided in Figure 3.10; in this case, it arises at the surface of a three-dimensional topological insulator. Topological aspects of such points in three dimensions are discussed in detail in Chapter 7.

One way to view the point made by Haldane is that there are inequivalent ways that a gap could open up at these band touchings, even if we preserve the size of unit cell. Let us first consider a trivial way to open up a band gap. If instead of graphene, which is a single layer of carbon atoms, we had a monolayer honeycomb material with different atoms on the two inequivalent sites (A and B in Figure 3.8), what would happen? Nature furnishes an example in boron nitride, BN. The boron and nitrogen orbitals would be expected to have different on-site energies, which means that the orbital energy is not just an overall constant that we can neglect. Instead the difference in orbital energies between A and B sites, $\Delta = \epsilon_A - \epsilon_B$, is an important parameter that affects the band structure. An energy gap opens at the $\mathbf{K}$ and $\mathbf{K}'$ points. This is not surprising and very similar in spirit to the opening of a gap in a one-dimensional tight-binding chain when odd and even atoms become inequivalent.

Haldane pointed out that a gap also opens when we add a kind of spatially variable magnetic field, even if the field averages to zero, and that the nature of the bands in this case is more topological. Suppose we add second-neighbor hopping,

and also a magnetic field that gives phases to second-neighbor hopping elements as shown in Figure 3.8. The precise form of this term is given below in Eq. 3.38, where a spin dependence is added in order to create a new phase. The total magnetic flux through each hexagon turns out to be zero, unlike for the Hofstadter model in Figure 3.5, and the original hoppings of strength t along nearest-neighbor bonds can remain unchanged. However, if there are additional processes such as second-neighbor hopping through the interior of the hexagons, these hoppings might be sensitive to the flux.

In the Haldane model, when a gap is present, the lower and upper bands have equal and opposite Chern numbers ± 1. If this material had the lower band filled and the upper band empty, it would support an integer quantum Hall effect, just as in the Hofstadter model with one band filled. The term Chern insulator is often used for this kind of IQHE phase appearing on a lattice in zero average field, as in the Haldane model with one band filled.

Even though the total field is zero, we can see that the Chern insulator phase in this model has some features reminiscent of the Hofstadter model. The second-neighbor hoppings used to open the gap have imaginary parts, so the Hamiltonian matrix is not purely real as it was for the simple band insulator case representing BN. The appearance of imaginary matrix elements is a sign that the Haldane model breaks the same kind of symmetry as an external magnetic field. We study this time-reversal symmetry in the next section by taking a step backward and starting with some simple pictures from classical physics.

3.3 Time-Reversal Symmetry in Classical and Quantum Physics

While symmetry is the bread and butter of large swaths of physics, time-reversal symmetry seems not to receive the attention it deserves in undergraduate classes. Here we use classical concepts to understand how standard observables transform under change of the sign of time, and then explain how its antiunitary nature makes time-reversal symmetry quite different from standard unitary symmetries at the quantum level.

To visualize time-reversal symmetry intuitively, consider running the slides of a film in reversed order. Then spatial directions are preserved but the sign of time has been flipped ($t \to -t$), and as a result, objects appear to move backward. If we think about the velocity $\frac{dx}{dt}$, then we would expect this to flip sign under either spatial inversion ($\mathbf{r} \to -\mathbf{r}$) or time-reversal. We say that the velocity is odd under each of these transformations, by analogy with an odd function on the line, which flips under $x \to -x$. The acceleration is odd under inversion but unchanged (even) under time-reversal, because it has two powers of inverse time.

https://doi.org/10.1017/9781316226308.004 Published online by Cambridge University Press

According to Newton, accelerations are induced by forces, so now let us think about the Lorentz force law

$$m\frac{d^2\mathbf{r}}{dt^2} = q(\mathbf{E} + \mathbf{v} \times \mathbf{B}). \tag{3.24}$$

Then, assuming mass and charge are unchanged under both symmetries, we conclude that electric field $\mathbf{E}$ is odd under inversion and even under time-reversal, while $\mathbf{B}$ behaves oppositely: magnetic fields are odd under time-reversal but even under inversion. (As an exercise, consider a loop of current producing a magnetic dipole, and verify that the direction of that dipole has the expected behavior under both symmetries.) It might seem unusual that magnetic materials break time-reversal symmetry spontaneously and hence can produce a magnetic moment, but recall that many other symmetries such as translational and rotational symmetries are routinely broken in the solid state.

We remark in passing that it can be dangerous to assume that both sides of an equation describing macroscopic behavior should transform identically under time-reversal, even if the underlying microscopic equations are time-reversal-invariant. Macroscopic systems in which we only study a subset of degrees of freedom have an entropic arrow of time: for example, we see entropy increase in our daily lives, even though the microscopic equations of motion are reversible. We think of this arrow of time as resulting from coarse graining, which means not being able to observe exactly what every particle of a large system is doing. Also, a remarkable discovery in high-energy physics is that the microscopic equations of our universe are actually not reversible (they break time-reversal symmetry), which one can see in the properties of unusual particles called kaons. But the equations for the particles that appear in solids do have this symmetry, while in magnetic solids, there is spontaneous breaking of this symmetry even though the underlying equations are time-reversal-invariant.

Time-reversal has an interesting effect in quantum mechanics when we think about spin-half particles like electrons. For such a particle, in a system with time-reversal symmetry like an atom in zero magnetic field, there are always degenerate eigenstates (Kramers pairs) for the following reason: every one-electron state is degenerate with, and different from, its time-reversed version. For integer-spin particles, a state can be the same as its time-reversed version, but this never happens for fermions (spin-half particles). Time-reversal symmetry is special in quantum mechanics because it is represented as an antiunitary operation (the product of complex conjugation and a unitary operation), while ordinary symmetries like rotations are unitary operations. Some intuition for why time-reversal must include a complex conjugation, and hence be antiunitary, comes from considering how complex conjugation, acting on the time-dependent Schrödinger equation, gives a

solution with the opposite sense of time, or noting that the time-reversed version of the wavefunction of a plane wave moving to the right, e^{ikx}, is just e^{-ikx}, which is also its complex conjugate. A 1931 theorem of Wigner implies that symmetries preserving all observables must be implemented in quantum mechanics by either unitary or antiunitary operators.

This fact might seem esoteric, but the time-reversal symmetry of electrons has been extremely important in some new discoveries in solids in the last decade or so. When an electric field is applied to an atom, or spin-orbit coupling is added, these twofold degeneracies do not split, but they do split when a magnetic field is added, which is a clue that magnetic fields behave differently and break time-reversal symmetry. The next section gives an intuitive picture of how the behavior of electrons under time-reversal, including the existence of Kramers pairs, gives rise to new states with directly measurable experimental consequences.

3.4 Topological Insulators in 2D: Basic Phenomena and Theory

Topological insulators in 2D and 3D result from the spin-orbit coupling intrinsic to all materials, rather than from external magnetic fields. For simplicity, consider an example of spin-orbit coupling familiar from atomic physics:

$$H_{SO} = \lambda \mathbf{L} \cdot \mathbf{S}, \tag{3.25}$$

where $\mathbf{L}$ is the orbital angular momentum of an electron, $\mathbf{S}$ is spin angular momentum, and λ measures of the spin-orbit coupling strength. This coupling arises because the electric field of the nucleus, when viewed in the frame of a relativistically moving electron, acquires a magnetic component that couples to the electron spin via the Zeeman effect. Because it is a relativistic effect, strong spin-orbit coupling requires fast-moving electrons and hence strongly charged nuclei: $\lambda \propto Z^4$ where Z is the atomic number of the nucleus.

In general, crystals have less symmetry than isolated atoms, and the form of spin-orbit coupling is less constrained. However, the spin-orbit force on an electron in a crystal depends on the electron's motion through space and in this sense is loosely similar to a magnetic field, which also generates a velocity-dependent force. More explicitly, think of a 2D electron moving in a constant magnetic field $B\hat{\mathbf{z}}$. Representing the magnetic field in the rotational gauge $\mathbf{A} = (-By/2, Bx/2, 0)$, the linear coupling to the electron is

$$\mathbf{A} \cdot \mathbf{p} = \frac{B}{2}(\mathbf{z} \times \mathbf{r}) \cdot \mathbf{p} = \frac{B}{2}\mathbf{L}_z, \tag{3.26}$$

so a magnetic field is also a coupling to orbital angular momentum. However, this similarity masks some clear differences, for example, the spin-orbit force changes

sign if the electron spin changes sign. This is a signal of a more fundamental difference: spin-orbit coupling preserves time-reversal symmetry (is even under time-reversal), unlike a magnetic field, because spin and orbital angular momentum are both odd under time-reversal. We will discuss time-reversal more formally in a moment because it is the key to the topological protection in topological insulators.

Another difference between spin-orbit coupling and a constant magnetic field is that spin-orbit forces in a crystal are expected to vary significantly on the scale of a unit cell. Before developing a theory of the IQHE in a periodic potential, let us state some of the basic phenomenology of the QSHE. If we could make two oppositely directed copies of the IQHE for up and down spins, for example, an $n = 1$ state for $S_z = +\hbar/2$ and an $n = -1$ state (i.e., oppositely directed effective magnetic field) for $S_z = -\hbar/2$, then this overall combination would have time-reversal symmetry, as time-reversal flips both the spin and the magnetic field. The resulting quantum Hall charge currents would cancel out, but there would be a quantized spin current (a quantum spin Hall effect) (Murakami et al., 2004):

$$\mathcal{J}^i_j = \sigma^s_H \epsilon_{ijk} E_k. \tag{3.27}$$

The spin current $\mathcal{J}$ carries two indices, one a spin direction and one a spatial direction, and σ^s_H is a quantized spin conductivity. We will not worry for the moment about the various subtleties of defining a spin current in a solid with spin-orbit coupling, but we will argue in a moment that there is in general no quantized spin transport of the form (3.27) along any spin axis.[5] The appearance of the electric field rather than the magnetic field in the quantum spin Hall equation results from the goal of having a potentially dissipationless current equation. If dissipation provides no arrow of time, then both sides should transform in the same way under the time-reversal operation, which fixes the field on the right side to be **E** rather than **B**.

In real materials, there is no conserved direction of spin like $\hat{\mathbf{z}}$ in this example, and it is an unphysical simplification to separate electrons into two independent species. Looking at the edge, one would expect naively that the two oppositely directed edge modes would mix with each other under realistic spin-orbit coupling and disorder, leading to localization and no propagating edge mode. This simple expectation turns out to be incorrect. Under some circumstances, a propagating edge mode does survive and distinguishes ordinary and topological 2D insulators. The key in understanding when spin-orbit leads to a protected edge state is to consider the action of time-reversal symmetry on electrons; this step is what makes the

[5] In mathematical terms, in realistic solids not only is spin rotational symmetry (SU(2)) broken, but there are no unbroken U(1) subgroups as crystals do not have continuous rotations around any axis. So there is no absolute conservation of spin because there is no continuous symmetry left to protect it, although spin can be approximately conserved for a relatively long time scale (greater than picoseconds) in some solids.

theory of the 2D topological insulator a highly nontrivial advance on the theory of the IQHE. One result is that, in the more topological language introduced below, 2D time-reversal-symmetric insulators are not characterized by an integer, but by a $\mathbb{Z}_2$ invariant that only takes two possible values: even, in ordinary insulators, and odd, in topological insulators.

We wish to explain the surprising fact that the quantum spin Hall phase survives, with interesting modifications, once we allow more realistic spin-orbit coupling, as long as time-reversal symmetry remains unbroken. The time-reversal operator $\mathcal{T}$ acts differently in Fermi and Bose systems, or more precisely in half-integer versus integer spin systems. Kramers showed that the square of the time-reversal operator is connected to a 2π rotation, which implies that

$$\mathcal{T}^2 = (-\mathbf{1})^{2S}, \tag{3.28}$$

where S is the total spin quantum number of a state: half-integer-spin systems pick up a minus sign under two time-reversal operations. For example, for a scalar wavefunction ($S = 0$) time-reversal is normally implemented simply as complex conjugation, which squares to the identity. For a single spin-half, a commonly used form is

$$\mathcal{T} = i\sigma^y K = \begin{pmatrix} 0 & 1 \\ -1 & 0 \end{pmatrix} K, \tag{3.29}$$

where σ^y is the Pauli matrix and K is complex conjugation. Then

$$\mathcal{T}^2 = \begin{pmatrix} 0 & 1 \\ -1 & 0 \end{pmatrix} K \begin{pmatrix} 0 & 1 \\ -1 & 0 \end{pmatrix} K = K^2 \begin{pmatrix} -1 & 0 \\ 0 & -1 \end{pmatrix} = -\mathbf{1}. \tag{3.30}$$

Note that the inverse of the time-reversal operator is thus $\mathcal{T}$ or $-\mathcal{T}$, depending on the spin.

A consequence of this is the existence of Kramers pairs: every eigenstate of a time-reversal-invariant spin-half system is at least twofold degenerate. In other words, every state of a spin-half particle is degenerate with *and distinct from* its time-reversed version, while an eigenstate of an integer-spin particle can be invariant under time reversal. We will show that a time-reversal invariant Hermitian operator H', which could be the system's Hamiltonian, is zero between the members of a Kramers pair, that is, a state ψ and its time-reversal conjugate $\phi = \mathcal{T}\psi$.

First, let us give the proper definition of an antiunitary operator. A unitary operator U is one that preserves inner products: $\langle U\phi|U\psi\rangle = \langle\phi|\psi\rangle$ for every pair of states ψ and ϕ, which yields the compact result $U^\dagger U = \mathbf{1}$ or $U^\dagger = U^{-1}$. To say that a Hamiltonian is invariant under U means that its matrix elements satisfy

$$\langle U\phi|H|U\psi\rangle = \langle\phi|H|\psi\rangle \Rightarrow U^\dagger H U = H. \tag{3.31}$$

https://doi.org/10.1017/9781316226308.004 Published online by Cambridge University Press

An antiunitary operator K involves complex conjugation, so we modify the above definition so that the effect of K on inner products includes a complex conjugation or reversal of order:

$$\langle K\phi|K\psi\rangle = \langle\phi|\psi\rangle^* = \langle\psi|\phi\rangle. \tag{3.32}$$

To check that this makes sense, take the Hilbert space to be scalar wavefunctions and allow K to be just complex conjugation. Now the statement that antiunitary operator K is a symmetry of Hamiltonian H is similarly modified to

$$\langle K\phi|H|K\psi\rangle = \langle\psi|H|\phi\rangle. \tag{3.33}$$

A useful alternate form of the statement that H has K as a symmetry comes from rewriting

$$\langle K\phi|H|K\psi\rangle = \langle K\phi|HK\psi\rangle = \langle K\phi|(KK^{-1})HK\psi\rangle = \langle K^{-1}HK\psi|\phi\rangle, \tag{3.34}$$

which becomes the above statement of time-reversal invariance if $K^{-1}HK = H$, that is, if H and K commute.

We now apply this rule with $K = \mathcal{T}$ to the matrix element between an eigenstate ψ and its time-reversal conjugate of a time-reversal-symmetric Hamiltonian H'. This leads to the first equality in

$$\langle\mathcal{T}\psi|H'|\psi\rangle = \langle\mathcal{T}\psi|H'|\mathcal{T}^2\psi\rangle = -\langle\mathcal{T}\psi|H'|\psi\rangle = 0. \tag{3.35}$$

The second step is just the fact that $\mathcal{T}^2 = -1$, and the last step is to note that the first and third entries are opposite each other, and if $x = -x$, then $x = 0$. Since H' is time-reversal invariant, $\mathcal{T}|\psi\rangle$ must be an eigenstate with the same energy as $|\psi\rangle$, and from the above it is a distinct, and in fact orthogonal, state.

We used the notation H' to stress that this result applies both to the original Hamiltonian and any perturbation respecting time-reversal symmetry. We immediately see that no mixing or scattering is induced between the two states of a Kramers pair; for example, the pair does not split into even and odd combinations with a gap, as one might have expected. Combining Kramers pairs with what is known about the edge state, we can say a bit about why an odd-even or $\mathbb{Z}_2$ invariant might be physical here. If there is only a single Kramers pair of edge states and we consider low-energy elastic scattering, then a right-moving excitation can only backscatter into its time-reversal conjugate, which is forbidden by the Kramers result above if the perturbation inducing scattering is time-reversal invariant. However, if we have two Kramers pairs of edge modes, then a right-mover can back-scatter to the left-mover that is *not* its time-reversal conjugate. This process will, in general, eliminate these two Kramers pairs from the low-energy theory.

Our general belief based on this argument is that a system with an even number of Kramers pairs at the edge will, under time-reversal-invariant backscattering,

https://doi.org/10.1017/9781316226308.004 Published online by Cambridge University Press

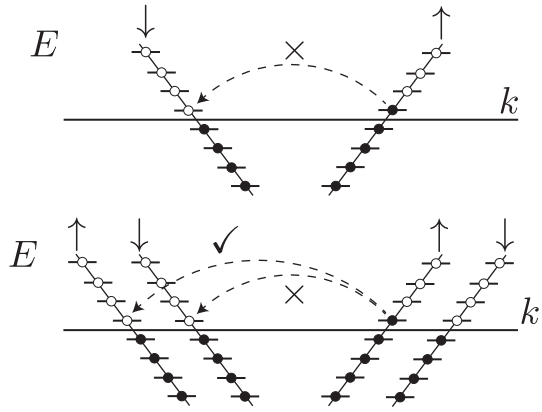

Fig. 3.6 Low-energy scattering processes at the edge of a 2D topological insulator (top), compared to those in an ordinary quantum wire (bottom). What is shown is the energy-momentum relation along the edge. Solid circles denote occupied states and open circles empty states. The lowest-energy current-carrying state (one extra electron moving right) has only a single decay process allowed by energy conservation, and Kramers's theorem prevents any time-reversal-symmetric perturbation from inducing this process because the two states involved are time-reversal conjugate, i.e., members of a Kramers pair. In the simplest case, they can be viewed as opposite spin, but the absence of scattering persists even with spin-orbit coupling as long as time-reversal is unbroken. In the ordinary wire (below), with an even number of Kramers pairs, there are two possible decay processes for the current-carrying state shown, and while one is forbidden by time-reversal symmetry, the other is allowed (check mark) and ultimately leads to localization.

localize in pairs down to zero Kramers pairs, while a system with an odd number of Kramers pairs will wind up with a single stable Kramers pair. In other words (Figure 3.6), an ordinary quantum wire with an even number of Kramers pairs is susceptible to localization, while the edge of a 2D insulator is "half of a quantum wire," and stable as long as $\mathcal{T}$ remains a good symmetry. It is as though we took a single quantum wire and separated it into two halves at two opposite edges of the 2D insulator, thereby making it stable to time-reversal-symmetric perturbations. The same concept is helpful in understanding the 3D topological insulator introduced below.

Additional support for this odd-even argument will be provided by our next approach. We would like, rather than just trying to understand whether the edge is stable, to predict from bulk properties whether the edge will have an even or odd number of Kramers pairs. Since deriving the bulk-edge correspondence directly is quite difficult, what we will show is that starting from the bulk T-invariant system, there are two topological classes. These correspond in the example above (of separated up- and down-spins) to paired IQHE states with even or odd Chern number

https://doi.org/10.1017/9781316226308.004 Published online by Cambridge University Press

for one spin. Then the known connection between IQHE integer and number of edge states is good evidence for the statements above about Kramers pairs of edge modes.

Before turning to the bulk, we sketch a graphical version of the original argument by Kane and Mele for why Kramers degeneracy means that there are two inequivalent possibilities for edge structure. Imagine a crystalline edge of a 2D insulator, that is, one at which periodicity is unbroken along the edge and Bloch's theorem applies in this direction (Figure 3.7). We can then view a system that is gapped in bulk as a one-dimensional band structure with a bandgap except possibly at the edge. A lattice system in an IQHE state, also known as a Chern insulator, will have at least one state in the gap at each edge reaching from the conduction band to the valence band, with a preferred direction.

Now consider what edge structures are allowed by time-reversal symmetry. The action of time-reversal symmetry on the Bloch Hamiltonians $H(\mathbf{k})$, whose eigenvalues are the energies of Bloch states at crystal momentum $\mathbf{k}$, in a

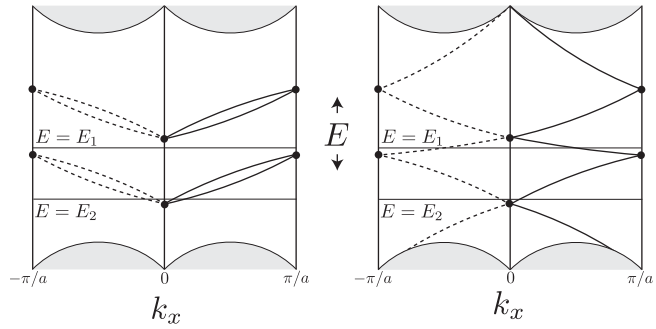

Fig. 3.7 Consider an edge of a semi-infinite two-dimensional insulator preserving lattice translational symmetry by distance a in the $\hat{\mathbf{x}}$ direction. The diagrams show two possible band structures in the resulting one-dimensional Brillouin zone. There are bulk states (shaded) from occupied (conduction) and unoccupied (valence) bands above and below the bulk bandgap. For states inside the bulk bandgap, there are two possible arrangements consistent with time-reversal symmetry, which requires Kramers degeneracies at momentum $k = 0$ and $k = \pm\pi/a$. The time-reversal symmetry means that $E(k) = E(-k)$ and drawing the $k \geq 0$ half is sufficient: the dashed bands are just reflected versions of the solid bands, so we could view the right half as an effective Brillouin zone. In an ordinary insulator (left), there can be edge states but their bands form loops, so that at some energies, such as energy E_1 in the diagram, there may not be any edge states, while at other energies such as E_2 in the diagram, there are an even number of Kramers pairs. Kane and Mele (2005b) pointed out another possibility: in the topological insulator (right), the two bands coming into one Kramers pair at $k_x = 0$ go into different Kramers points at $k_x = \pi/a$. This forces a zigzag pattern and an odd number of Kramers pairs at every energy in the bulk bandgap.

https://doi.org/10.1017/9781316226308.004 Published online by Cambridge University Press

time-reversal-invariant system is as follows: with Θ the representation of $\mathcal{T}$ in the Bloch Hilbert space,

$$\Theta H(\mathbf{k})\Theta^{-1} = H(-\mathbf{k}). \tag{3.36}$$

In words, the time-reversal operator acts both on the Bloch Hamiltonian and also on crystal momentum $\mathbf{k}$. In particular, only the time-reversal invariant momenta at which $\mathbf{k} = -\mathbf{k}$ are forced to have Kramers pairs. In one dimension there are just two such points, $k = 0$ and $k = \pm\pi/a$, recalling that crystal momenta are only defined modulo a reciprocal lattice vector. This combined action is one reason why more than two decades elapsed between the discovery of the integer-valued topological invariant that underlies the IQHE and the discovery of the $\mathbb{Z}_2$ invariants in time-reversal-invariant systems. The mathematical expression of those invariants in two and three dimensions is described starting in Section 4.4. Figure 3.7 gives the original picture of Kane and Mele for how this requirement leads to two distinct possibilities consistent with time-reversal invariance.

3.5 A Lattice Model of the 2D Topological Insulator

Returning to the idea of two copies of the IQHE generated by spin-orbit coupling, consider the model of graphene introduced in Kane and Mele (2005a). This is a tight-binding model for independent electrons on the honeycomb lattice (Figure 3.8). The spin-independent part of the Hamiltonian consists of a nearest-neighbor hopping, which alone would give a semimetallic spectrum with Dirac nodes at certain points in the 2D Brillouin zone, plus a staggered sublattice potential whose effect is to introduce a gap:

$$H_0 = t \sum_{\langle ij\rangle\sigma} c^\dagger_{i\sigma} c_{j\sigma} + \lambda_v \sum_{i\sigma} \xi_i c^\dagger_{i\sigma} c_{i\sigma}. \tag{3.37}$$

Here $\langle ij\rangle$ denotes nearest-neighbor pairs of sites, σ is a spin index, ξ_i alternates sign between sublattices of the honeycomb, and t and λ_v are free parameters.

The insulator created by increasing λ_v is an unremarkable, spin-independent band insulator. However, the symmetries of graphene also permit an intrinsic spin-orbit coupling of the form

$$H_{SO} = i\lambda_{SO} \sum_{\langle\langle ij\rangle\rangle\sigma_1\sigma_2} \nu_{ij} c^\dagger_{i\sigma_1} s^z_{\sigma_1\sigma_2} c_{j\sigma_2}. \tag{3.38}$$

Here $\nu_{ij} = [(2/\sqrt{3})\hat{\boldsymbol{d}}_1 \times \hat{\boldsymbol{d}}_2]_z = \pm 1$, where i and j are next nearest neighbors and $\hat{\boldsymbol{d}}_1$ and $\hat{\boldsymbol{d}}_2$ are unit vectors along the two bonds that connect i to j. Here s^z is the matrix representation of the spin operator, that is, $\hbar\sigma^z/2$. Including this type of spin-orbit coupling alone would not be a realistic model. For example, the

https://doi.org/10.1017/9781316226308.004 Published online by Cambridge University Press

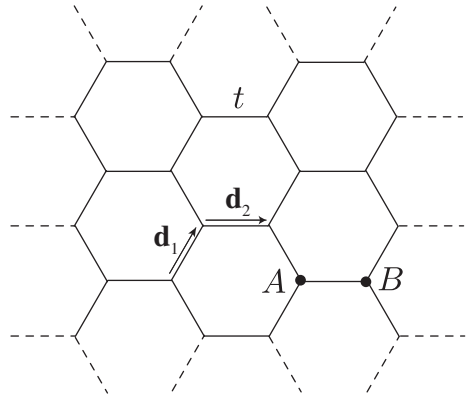

Fig. 3.8 The honeycomb lattice used to model graphene (see also Section 2.5) and to define the tight-binding models of Haldane (1988) and of Kane and Mele (2005a). With just nearest-neighbor hopping t, this provides a commonly used model of graphene, with gapless Dirac points at two inequivalent points in the Brillouin zone. A simple band gap respecting time-reversal and spin symmetries would be created if we allowed different on-site potentials on the A and B sublattices; one site on each sublattice is indicated. Adding second-neighbor hoppings gives the possibility of opening a gap between topologically nontrivial bands. For the two sites connected by the sum of the vectors $\mathbf{d}_1$ and $\mathbf{d}_2$, the factor ν_{ij} of Eq. 3.38 is $\nu_{ij} = [(2/\sqrt{3})\hat{\boldsymbol{d}}_1 \times \hat{\boldsymbol{d}}_2]_z = -1$.

Hamiltonian $H_0 + H_{SO}$ conserves S_z, the distinguished component of electron spin, and reduces for fixed spin (up or down) to the model introduced by Haldane for a lattice quantum Hall effect (Haldane, 1988). Generic spin-orbit coupling in solids should not conserve any component of electron spin.

As a test of what happens when S_z is not conserved, consider the addition of Rashba-type spin-orbit coupling:

$$H_R = i\lambda_R \sum_{\langle ij\rangle\sigma_1\sigma_2} c^\dagger_{i\sigma_1} \left(\boldsymbol{s}_{\sigma_1\sigma_2} \times \hat{\boldsymbol{d}}_{ij}\right)_z c_{j\sigma_2}, \tag{3.39}$$

with $\boldsymbol{d}_{ij}$ the vector from $i \to j$ and $\hat{\boldsymbol{d}}_{ij}$ the corresponding unit vector, and the spin operators $\mathbf{s}$ now involve all three of the Pauli matrices. Note that Rashba spin-orbit coupling is not intrinsic to graphene but generated by an inversion-symmetry breaking field, such as an electric field, in the out-of-plane direction (Bychkov and Rashba, 1984). (Inversion means the symmetry $\mathbf{r} \to -\mathbf{r}$ introduced in Section 3.3.) The Rashba coupling is a standard form, discussed in more detail around Eq. 3.40, that is believed to be a reasonable model for the dominant spin-orbit coupling in adsorbed graphene.

A topological phase survives, but is strongly modified by the Rashba term, consistent with the physical picture of even and odd classes above. For a system with

https://doi.org/10.1017/9781316226308.004 Published online by Cambridge University Press

S_z conserved, there are many phases labeled by an integer n, as in the IQHE: if spin-up electrons are in the $\nu = n$ state, then spin-down electrons must be in the $\nu = -n$ state by time-reversal symmetry, where the sign indicates that the direction of the effective magnetic field is reversed. Once S_z is not conserved because $\lambda_R \neq 0$, there are only two categories, the ordinary and topological insulators. The decoupled $\nu = \pm n$ cases with S_z conserved can be adiabatically connected (i.e., without closing the gap), once S_z is not conserved, to the ordinary insulator for even n and to the topological insulator for odd n, at least once disorder is allowed. This continuity is described using properties of band structures in Section 4.4.

This completes our outline of two-dimensional insulating systems. This kind of topological insulator was observed by a transport measurement in (Hg,Cd)Te quantum wells (Koenig et al., 2007), building on an analysis in terms of the Bernevig-Hughes-Zhang tight-binding model (Bernevig et al., 2006). A simplified description of this experiment is that it observed, in zero magnetic field, a two-terminal conductance $2e^2/h$, consistent with the expected conductance e^2/h for each edge if each edge has a single mode, with no spin degeneracy. More recent work has observed some of the predicted spin transport signatures as well, although as expected the amount of spin transported for a given applied voltage is not quantized, unlike the amount of charge. Some intuition for why this particular material shows the quantum spin Hall effect is provided by noting that strained HgTe is an inverted band gap semiconductor: one can imagine that as spin-orbit coupling increases a band moves from the conduction band to the valence band. This is not alone sufficient for the topological phase, as an even number of band inversions would return the system to the ordinary class (as is believed to happen in PbTe), but in HgTe calculations of the type described in Chapter 4 show that material is indeed topological.

3.6 3D Topological Insulators: Basic Phenomena

The notion of a 2D topological insulator as having half of a quantum wire at each edge leads naturally to a 3D generalization, and this 3D topological insulator phase has seen an explosion of interest since its experimental observation in 2008. The existence of a 3D topological phase came as something of a surprise, as the integer quantum Hall effect was known not to have a genuinely 3D analogue: a three-dimensional system in a magnetic field can in principle be put into layered quantum Hall states, with chiral metals on their sides (Chalker and Dohmen, 1995). In this section we sketch a picture of the 3D topological phase and some of its key properties, particularly its surface state, deferring a full theoretical analysis of the bulk until the following chapter. For readers preferring a tight-binding model like the above, it is possible to imitate the two-dimensional case by starting from a bulk

semimetal, namely, the tight-binding model on the diamond lattice, and adding an appropriate spin-orbit term to open a topological gap (Fu et al., 2007).

Let us start by trying to create a surface state that is half of an ordinary 2D metal, in the same way as we previously were led to consider half of a spin-independent quantum wire. In the wire, we can count branches of the energy-momentum relation as in Figure 3.6. At a surface, we instead count sheets of the Fermi surface. To understand what this means, start by thinking about an ordinary 2D metal with time-reversal symmetry. Consider a Hamiltonian consisting of a quadratic spin-independent part and a Rashba spin-orbit part:

$$H = \frac{p^2}{2m} + \lambda(\mathbf{p} \times \boldsymbol{\sigma})_z. \tag{3.40}$$

The effect of the Rashba term is to spin-split the Fermi surface; the energy-momentum plot along a line of momenta in the 2D Brillouin zone now has the form of two displaced parabolas (Figure 3.9). However, at every energy the Fermi surface still consists of an even number of sheets (either two or zero), which in this case are circles. We could equally well, for the purposes of this discussion, consider Dresselhaus spin-orbit coupling of the form $\mathbf{p} \times \boldsymbol{\sigma}$, which would also lead to two sheets of the Fermi surface, now with inward-directed and outward-directed spins.

It is believed that any strictly two-dimensional band structure with time-reversal symmetry will have this property: including spin, the Fermi surface contains an even number of sheets. We could break time-reversal symmetry by applying

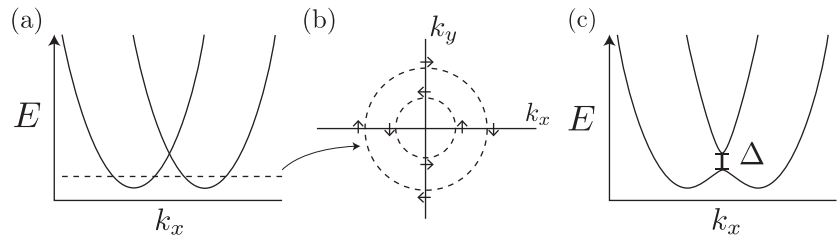

Fig. 3.9 Band structure of a two-dimensional electron gas with Rashba spin-orbit coupling (Eq. 3.40). (a) Energy-momentum relation along a cut with $k_y = 0$: the bands consist of two displaced parabolas describing opposite spin states. Note that opposite momenta will have opposite spin states as required by time-reversal symmetry. (b) At a generic value of Fermi energy (dotted line) above the band minimum, the Fermi surface consists of two sheets, which for this model are circles around which the spin direction precesses. (c) Applying a Zeeman magnetic field $h\sigma_z$ is one way to break time-reversal symmetry: it induces a gap Δ at $\mathbf{k} = 0$ of magnitude proportional to h, and for energies in this gap, there is only a single Fermi surface sheet.

https://doi.org/10.1017/9781316226308.004 Published online by Cambridge University Press

a Zeeman magnetic field, as shown in Figure 3.9b. Now consider instead the linear-in-momentum Hamiltonian

$$H = \lambda(\mathbf{p} \times \boldsymbol{\sigma})_z. \tag{3.41}$$

This Hamiltonian is not bounded below, so we would not accept it as the ultimate Hamiltonian of a system, but it is nevertheless a reasonable description of the surface states in a bulk band gap of a topological insulator (Figure 3.10). The relativistic dispersion relation with zero effective mass is similar to that in graphene, which is a strictly 2D material (a layer of carbon atoms, whose low-energy electronic structure is well described by a nearest-neighbor tight-binding model on the honeycomb lattice discussed in this and the previous chapter).

However, graphene has such a relativistic dispersion relation around the *two* inequivalent Dirac points, $\pm\mathbf{K}$, in the Brillouin zone, Section 2.5.1. It also has a twofold spin degeneracy at each value of momentum if spin-orbit coupling is neglected, and weak spin-orbit coupling splits this degeneracy but keeps the number of sheets of the Fermi surface even. Having an odd number of sheets of the Fermi surface with time-reversal symmetry is the defining feature of the 3D TI surface state, which appears at the boundary between two topologically inequivalent bulk band structures (e.g., a TI material and vacuum). Another way this difference is stated is that in a 3D TI surface state, the Fermi surface encloses an odd number of Dirac points, while in a generic 2D system it encloses an even number. One reason that one- or two-dimensional systems with an odd number of Fermi surface sheets are interesting, whether arising either via topology or via an applied magnetic field, is that they can serve as precursors for topological superconductivity as discussed in Chapter 9.

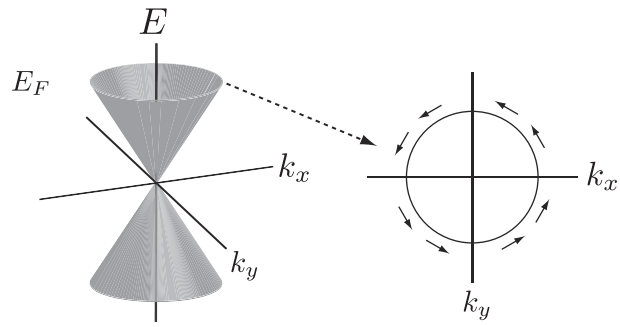

Fig. 3.10 Simplified band structure of a 3D topological insulator. The Dirac cone of surface states (left) terminates above and below in bulk electronic states. Only the surface states associated with one surface are shown, and there is a single spin direction at each value of momentum. There is a single Fermi surface sheet in the bandgap. Angle-resolved photoemission spectroscopy of Bi_2Se_3, showing this structure within the bandgap, is shown in Figure 1.2.

https://doi.org/10.1017/9781316226308.004 Published online by Cambridge University Press

Just as in the two-dimensional case, there is an odd-even effect. One topological insulator surface in isolation cannot be localized by disorder that respects time-reversal; it can be viewed as an ordinary two-dimensional metal which was stabilized by being split into two halves. However, two surfaces hybridized together, as in a thin film, can localize or develop a gap and are not very different from a normal two-dimensional metal with strong spin-orbit coupling. The "factor of 2" difference between a topological insulator surface state and a standard 2D metal, in the sense of having one Dirac cone or two, respectively, has remarkably far-reaching consequences beyond the stability to disorder. Three examples that will appear later in this book are the quantized magnetoelectric effect, unusual magnetotransport phenomena, and novel superconducting proximity effects.

As in the two-dimensional case, these properties emerge from a bulk topological invariant of $\mathbb{Z}_2$ type. Strictly speaking there are four bulk invariants of a 3D time-reversal-invariant band structure (Moore and Balents, 2007; Fu et al., 2007; Roy, 2009), of which three correspond to layered versions of the 2D topological insulator and the fourth is genuinely three-dimensional and responsible for the surface state described here. We postpone the analysis of the bulk invariants to Chapter 4 because they are substantially more complicated than the two-dimensional case. In the two-dimensional case, we could get into the topologically nontrivial phase by essentially separating electrons into up spin and down spin, with S_z commuting with the Hamiltonian. Then two oppositely directed copies of the IQHE provided a simple realization of the quantum spin Hall state or 2D topological insulator, and the challenge was to show that this state is stable to more realistic spin-orbit coupling. In three dimensions, getting into the fully 3D topological phase requires starting with the vector nature of spin-orbit coupling from the very beginning, as no model with S_z conservation realizes the nontrivial value of the invariant (Chapter 4).

Since time-reversal symmetry is required for the topological insulator phase to be well defined, it is natural to ask how the odd-even distinction is violated by breaking time-reversal. Adding a small Zeeman magnetic field $h\sigma_z$ to the Hamiltonian in (3.40) opens up a gap at the Γ point ($\mathbf{p} = 0$) but not elsewhere, meaning that there is now a range of energies with a single sheet of the Fermi surface. This effect is visible in transport measurements (Quay et al., 2010) and has become very important as a means to replicate some of the physics of topological insulator surface states in the quest to create unconventional superconductors with Majorana excitations (Chapter 9).

What about adding a magnetic field to the model topological insulator surface state Hamiltonian (3.41)? Remarkably, starting with one Dirac cone and applying a strong magnetic field gives a half-integer quantum Hall effect

$$\sigma_{xy} = (n + 1/2)e^2/h, \quad n \in \mathbb{Z} \tag{3.42}$$

https://doi.org/10.1017/9781316226308.004 Published online by Cambridge University Press

rather than an integer quantum Hall effect, so the odd numbers of Dirac fermions at the surface of a 3D topological insulator mean that the overall surface Hall effect is half-integer (Fu and Kane, 2007). This might seem of minor interest as the two surfaces measured in parallel in an experiment on a slab will still give an integer result overall. However, understanding the deeper significance of this surface half-integer led to both a more general picture of the topological insulator phase and a better understanding of magnetoelectric effects in all materials.

While the quantum Hall effect was defined in terms of an observable physical response (the Hall effect) that is independent of whether the underlying system is made up of independent or interacting electrons, the band-structure definitions of the topological insulator are based on an independent-electron picture. However, the half-quantized surface Hall effect is a valid characterization of the phase by observable quantities. It is nevertheless more subtle than the quantum Hall effect, which is a property of the unperturbed system, because here a time-reversal-breaking perturbation was required to put the surface state in the quantum Hall regime.

As motivation for the reader to invest in learning the theoretical underpinnings covered in Chapter 4, here are a few questions raised by the above physical pictures of the surface. We emphasized that the edge states and surface states that were the focus of this chapter are independent of surface details, so they must be forced to exist by some bulk property. What bulk property determines whether a given material falls in the topological or ordinary category? The answer in every case is a topological invariant, which can be expressed as an integral of the Berry phase of the electron wavefunctions. That raises the question of what physical significance these integrals might have when they are not quantized, for example, for the partially filled bands of a metal. Often that physical significance turns out to be related to the basic question of how the topological phases discussed in this chapter, and even ordinary nontopological materials, respond to applied electromagnetic fields.

3.7 Skyrmions in the Quantum Hall Effect

The physics of skyrmions in spin-polarized quantum Hall states lies at the intersection of several threads of this book. They appear as excitations of a phase which displays at the same time topological and conventional order; they generate a Berry flux through a twist of an internal order parameter; and they are themselves topological objects. Hence their study combines many of the concepts introduced in Chapter 2. They are also unusual in that they were theoretically predicted to exist (Sondhi et al., 1993) before their experimental discovery (Barrett et al., 1995),

a situation which was (and is) not all that common in quantum Hall physics, for the reasons discussed in Section 5.1.

3.7.1 Multicomponent Quantum Hall Systems and Flat-Band Ferromagnetism

In the case of electrons with an internal degree of freedom, such as its spin, there is a copy of each Landau level for each internal state. Even in the case of vanishing Zeeman coupling, when there are separate identical Landau levels for each spin direction, a filled Landau level ($\nu = 1$) is a ferromagnet and hence spontaneously breaks spin rotational symmetry, for reasons which we discuss in the following paragraphs. The SU(2) invariance of a vanishing Zeeman splitting despite the presence of a strong applied field in the quantum Hall regime is not as outlandish as it sounds. This can happen because the Zeeman coupling $g^*\mu_B B$ can vanish as a result of the vanishing effective electronic g-factor g^*. Often quite small at the outset, it can even be arranged to vanish exactly in some semiconductor heterostructures by applying external pressure, which changes g^* as a result of spin-orbit coupling.

The origin of this ferromagnetism is conceptually very simple, following from Pauli's principle that the a many-body wavefunction of fermions must be antisymmetric under particle exchange. Consider a pair wavefunction, written as a product of spatial and spin wavefunctions:

$$\Psi_{\sigma_1,\sigma_2}(\mathbf{r}_1, \mathbf{r}_2) = \psi_{\sigma_1,\sigma_2} \otimes f(\mathbf{r}_1 - \mathbf{r}_2) \otimes F(\mathbf{r}_1 + \mathbf{r}_2), \tag{3.43}$$

where the center of mass wavefunction F is unimportant for interaction effects. Choosing an antisymmetric relative spatial wavefunction f suppresses the probability for two electrons to be near each other, as it vanishes for vanishing separation $\mathbf{r}_1 - \mathbf{r}_2$. In the presence of a repulsive Coulomb interaction, this is energetically favorable. To keep the total wavefunction antisymmetric then requires a symmetric spin wavefunction ψ_{σ_1,σ_2}. This is just the triplet, that is, a wavefunction corresponding to total spin $S_{\text{tot}} = 1$, while the singlet $S_{\text{tot}} = 0$ is antisymmetric under particle exchange.

The reason this is called flat band ferromagnetism is that putting a node into a spatial wavefunction normally exacts a *kinetic* energy cost – just recall a particle in a box, the energy of an eigenfunction of which grows with the number of its nodes. For this reason, the majority of magnetic compounds are in fact antiferromagnets.

Here, this is different as the special feature of quantum Hall systems is their Landau level structure – all wavefunctions in a Landau level have the same kinetic energy, and hence the node can be put in without a kinetic energy penalty. Another familiar example, incidentally, of Coulomb-driven ferromagnetism is encoded in one of Hund's rules, stating that electrons in a partially filled shell of an atom, that

is, all of which occupy symmetry-related orbitals with the same kinetic energy, have their spins aligned.

3.7.2 Exchange-Enhanced Zeeman Splitting

A more detailed discussion of the two-particle problem is given in the section of the fractional quantum Hall effect (Section 5.1). In particular, the above argument would of course demand the pair wavefunction not just to vanish linearly but with a power as high as possible. For $\nu = 1$, the highest possible power, however, turns out to be 1, hence the ferromagnetism is captured correctly by this picture. In the absence of an internal degree of freedom, a filled Landau level of noninteracting electron gives rise to an incompressible state, that is, a state at which the chemical potential jumps as a function of filling on account of the cyclotron gap $\hbar\omega_c$. By contrast, for electrons with an internal degree of freedom, such as a spin, a priori no such gap exists. This happens only once the Landau level for each flavor (say, up and down spin) are filled. Thus, in the presence of flat-band ferromagnetism for interacting electrons, the system will be gapless at $\nu = 1$ for SU(2) spin symmetry (i.e., $E_Z = 0$) on account of the Goldstone mode corresponding to global rotations of the orientation of the ferromagnetic order.

The long-wavelength description of such a ferromagnet in a field is provided by a nonlinear σ-model (see also Eq. 2.70) based on the order parameter manifold, as introduced in Chapter 2. This is supplemented by a Zeeman energy term due to the applied field:

$$E = E_\sigma + E_Z = \frac{\rho_s}{2} \int d^2r |\nabla \mathbf{m}|^2 - g^* \mu_B B \nu \int d^2r\, m^z. \tag{3.44}$$

Here, the stiffness arises exclusively from the electron interactions. Analogously to the steps in Section 5.1.3 one finds in the lowest Landau level that

$$\rho_s = \sum_{q \neq 0} V(q) |q^2| \exp(-|q|^2/2) \tag{3.45}$$

is given solely in terms of the Fourier transform $V(q)$ of the electrons' real space interaction potential, $\mathcal{V}(r)$.

In the presence of a symmetry-breaking field, $g^* \neq 0$, the Zeeman splitting, $g^* \mu_B B$ per electron, and therefore the energy gap between spin-split Landau levels, is therefore enhanced by the exchange field, $\propto \rho_s$, of the neighboring aligned spins.

The nonlinear σ-model describes ferromagnetic spin wave excitations, including a gapless Goldstone mode for $g^* = 0$: the universal properties are in the first instance those of an ordinary ferromagnet. However, things will turn out to be much richer as the topological structures of the quantum Hall problem stabilize an excitation topologically distinct from spin waves.

https://doi.org/10.1017/9781316226308.004 Published online by Cambridge University Press

3.7.3 Skyrmions: Charged Topological Spin Textures

An interaction-generated gap in common parlance is taken as the feature distinguishing the FQHE from the IQHE. In that sense, for a multicomponent system, $\nu = 1$ can be thought of as a FQHE as the gap is eventually an interaction effect: in the presence of spontaneous symmetry breaking, otherwise negligible anisotropies become important. This has led to the statement that, as far as the QHE at $\nu = 1$ is concerned, "one is a fraction, too."

So, what is the nature of the charged excitations? These can take the form of skyrmions, topologically stable spin textures whose name was imported from Skyrme's model in nuclear physics.

The starting observation explaining the appearance of skyrmions is that the quantum Hall effects tend to occur whenever flux and charge are commensurate, that is to say when ν is an integer or a simple rational number (this notion will be made more concrete in the framework of Chern–Simons theory in Chapter 6). Therefore, starting from a quantum Hall state, adding or removing a charge interferes with this commensurability, and the system is left with an excitation.

As we discuss next, the topological charge of the skyrmion can be used to reestablish the commensurability in an elegant way. To see this, let us first present a topological classification of excitations of a ferromagnet in $d = 2$, which can be done using the tools developed in Section 2.7.3. Imposing the "compactifying" boundary condition that, infinitely far from the origin, all the spins point along a given direction, amounts to identifying all points "at infinity," or alternatively turns the infinite plane R^2 into the two-dimensional surface of a sphere, S^2. In Figure 3.11, the spin direction "at infinity" is chosen to be along the applied field if one is present, in order to maintain a finite Zeeman energy.

The order parameter manifold – the set of directions in which the magnetization vector $\mathbf{m}$ can point – itself can be described as the surface of a sphere as in Section 2.6. Hence, homotopy theory tells us that the possible order parameter configurations can be classified by an integer topological invariant n_Q of mapping from the surface of a sphere to itself:

$$\pi_2(S^2) = \mathbb{Z}. \tag{3.46}$$

A change in the local orientation of $\mathbf{m}$ induces a Berry flux in the following way. Imagine an electron moving in the plane, with its spin adiabatically following the local magnetization direction. The spin direction of the electron thus describes a trajectory on the sphere, just as described in Section 2.1, and the electron is thus subject to a Berry connection $\mathcal{A}$, generated by the spin texture, in addition to the vector potential A of the applied magnetic field. The Berry connection from the spin texture and the vector potential of the applied magnetic field are not just

https://doi.org/10.1017/9781316226308.004 Published online by Cambridge University Press

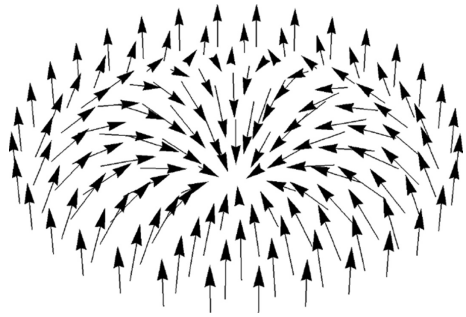

Fig. 3.11 A magnetic skyrmion is a texture in two space dimensions of a three-dimensional magnetization field. The magnetization at the center of the skyrmion points in a direction opposite to the distant points "at infinity." In between, the direction changes smoothly, tilting away from the vertical axis along radial directions, and winding like an XY vortex in the horizontal plane in the azimuthal direction.

analogous but combine to affect the electron in effectively the same way, since rotating the direction of spin around a closed path produces exactly the same U(1) phase effect on the wavefunction as moving the electron around a real-space path in a field.

The quantum Hall ferromagnet thus has the option of reinstating flux-charge commensurability by generating a texture in $\mathbf{m}$ so that the total charge precisely equals

$$Q = \nu \int d^2r \; \nabla \times (\mathcal{A} + A). \tag{3.47}$$

(Note that in $2d$, a magnetic field, being the curl of a two-component vector potential, is a pseudoscalar and can thus be identified with a charge.) The topological charge described above is thence simply proportional to the total electronic charge of the spin texture. In particular, (anti-)skyrmions have topological charge ± 1; skyrmions can reinstate the commensurability required by the topological nature of the QHE thanks to the – conceptually entirely separate – topological stability of their charge.

None of these topological considerations address issues of energetics, that is, the question which charged excitation is actually the cheapest. For quantum Hall skyrmions, there are three contributions which need to be considered in the first instance: the cost of the twist E_σ, and the Zeeman anisotropy cost E_Z from Eq. 3.44, as well as the Coulomb energy E_Q of the charge distribution $Q(r) = \nu \nabla \times \mathcal{A}(r)$.

Of all the possible topologically equivalent spin textures, an entire family gives a minimal $E_\sigma = 4\pi\rho_s$, namely, those which can be parameterized by spinors c

https://doi.org/10.1017/9781316226308.004 Published online by Cambridge University Press

(such that $\mathbf{m} = c^\dagger \boldsymbol{\sigma} c$, $\boldsymbol{\sigma}$ being the vector of Pauli matrices), whose entries are holomorphic functions:

$$c(z) = \begin{pmatrix} f(z) \\ g(z) \end{pmatrix}, \tag{3.48}$$

where $f(z)$ and $g(z)$ have n_Q zeroes each, and $\lim_{z\to\infty} f(z)/g(z) = 0$ imposed by our boundary condition. Placing the zero of $f(z)$ at the origin, and that of $g(z)$ at $z = \infty$, yields a charge $n_Q = 1$ skyrmion sketched in Figure 3.11:

$$c = \begin{pmatrix} \lambda \\ z \end{pmatrix}, \tag{3.49}$$

where λ parameterizes the "size" of the skyrmion in the sense that the spins point in the plane perpendicular to the quantization direction at a distance of λ from the origin.

While the Coulomb repulsion is optimized for a charge which is maximally spread out, the Zeeman energy favors compact skyrmions, as these involve flipping spins over a smaller area. The trade-off between these yields a texture which is no longer perfectly holomorphic.

In experiment, the net polarization of the electron system can be probed by nuclear magnetic resonance (NMR). For the GaAs quantum wells on which the first such experiments were done, the Knight shift of a ^{71}Ga nucleus is sensitive to the electronic spin polarization via a hyperfine interaction. It can thus probe the

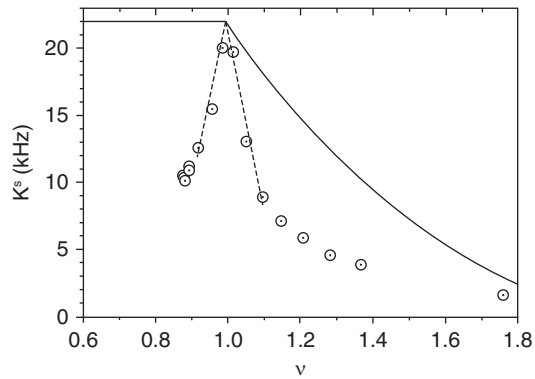

Fig. 3.12 The Knight shift K^s as a function of filling factor ν in a GaAs quantum well (Barrett et al., 1995). The fitted dashed line corresponds to a particles with 3.6 times the spin of a noninteracting electronic quasiparticle, denoted by the solid line. This indicates the presence of extended topological spin textures, skyrmions, as low-energy excitations near $\nu = 1$. Reprinted with permission by *Physical Review*.

https://doi.org/10.1017/9781316226308.004 Published online by Cambridge University Press

reduction of the magnetization density due to the excitations forced into the system by deviating from filling $\nu = 1$.

Thus, it was inferred that the effective spin of an excitation is about 3.6 times that of a noninteracting electron, as depicted in Figure 3.12. This confirmed the prediction that skyrmions are indeed the relevant low-energy excitations in this regime.